Room Temperature Spin Kondo Effect and Intermixing in Co/Cu Non-Local Spin Valves

J.D. Watts[1,2], J.S. Jeong[2], L. O'Brien[2,3], K.A. Mkhoyan[2], P.A. Crowell[1] and C. Leighton[2]

[1]School of Physics and Astronomy, University of Minnesota, Minneapolis, Minnesota, 55455, USA

[2]Department of Chemical Engineering and Material Science, University of Minnesota, Minneapolis, Minnesota, 55455, USA

[3]Department of Physics, University of Liverpool, Liverpool L69 3BX, UK

The anomalous low temperature suppression of the spin accumulation signal ΔR_{NL} in non-local spin valves (NLSVs) based on common ferromagnet (FM) / normal metal (N) pairings has recently been shown to result from a manifestation of the Kondo effect. Local magnetic moments in the N due to even minor levels of FM/N interdiffusion depolarize the injected spin current, suppressing the effective spin polarization around and below the Kondo temperature T_K. Previous studies have focused on FM/N combinations that happen to have low T_K, so that Kondo effects occur only well below 300 K. Here, we study NLSVs based on Co/Cu, a materials combination that is not only technologically relevant but also has a high T_K, up to 500 K. Despite the negligible *equilibrium* solubility of Co in Cu, we find clear Kondo effects in both ΔR_{NL} and the Cu resistivity, due to Co/Cu intermixing that we probe *via* quantitative transmission electron microscopy. Most significantly, under certain conditions the spin Kondo effect suppresses the injected spin polarization *even at room temperature,* with important technological implications. Studies *vs*. Cu thickness and annealing temperature reveal complex trends in interdiffusion lengths and Kondo effects, which we interpret in terms of the interplay between diffusion kinetics and thermodynamics, as well as the thickness dependence of the Kondo effect.

Corresponding author's email: leighton@umn.edu

Nonlocal spin valves (NLSVs)[1,2] efficiently separate charge and spin currents, allowing for the study of a wide variety of spin transport phenomena. These devices are also of interest for application as magnetic field sensors in hard disk drives, with several potential advantages over tunneling magnetoresistance devices.[3–5] In essence, an NLSV is simply a non-magnetic (N) channel connecting two ferromagnetic (FM) electrodes separated laterally by a distance d. A spin-polarized charge current I through one FM/N contact leads to a non-equilibrium spin accumulation in the N, and a corresponding non-local voltage ΔV_{NL} at the second contact, where ΔV_{NL} is determined by toggling the relative magnetizations of the two electrodes. A long-standing puzzle in metallic NLSVs has been the widely observed suppression of the spin accumulation signal $\Delta R_{NL} = \Delta V_{NL}/I$ at low temperatures (T) for common FM/N pairings, $i.e.$, non-monotonic $\Delta R_{NL}(T)$.[6–18] This is in apparent contrast to predictions based on Elliot-Yafet (EY) spin relaxation in pure N metals with low spin-orbit coupling,[19–21] where the spin relaxation time, and hence ΔR_{NL}, should increase monotonically on cooling.

Recent work has shown that the suppression of ΔR_{NL} at low T is due to FM impurities forming local moments in the N,[11] the resulting Kondo relaxation leading to depolarization of the injected spin current. This depolarization increases logarithmically on cooling through the Kondo temperature T_K [22] of the FM/N pair. This manifestation of the Kondo effect has now been observed in NLSVs in which the Kondo impurities diffuse into the N from the FM contacts,[11,13] as well as those in which the magnetic impurities are introduced throughout the N channel.[12,16] In the former case, local moments near the interface reduce the polarization α of the injected current. This can be quantitatively described by an extension of the Valet-Fert model accounting for spin relaxation at local moments.[23] In the latter case, local moments throughout the N lead to additional "bulk" spin relaxation, reducing the spin diffusion length λ_N. The Kondo-induced non-monotonicity in $\Delta R_{NL}(T)$ can be eliminated by using an N material incapable of supporting local moments for transition metal FMs,[11] such as Al,[22,24,25] or by inserting a thin layer of such a material at the FM/N interface.[11]

In this work we explore these "spin Kondo effects" (by which we mean T-dependent suppressions of the effective polarization or spin diffusion length by Kondo spin relaxation at magnetic impurities) in NLSVs fabricated from Co/Cu, an FM/N pairing that has not yet received detailed examination. This is despite the technological relevance of this pairing, which arises due to the widespread use of Cu as an N layer in spintronic devices, and the high Curie temperature, spin polarization, and anisotropy of Co-based alloys. More important in the current context, Co in Cu possesses a T_K of 500 K, $i.e.$, well above ambient.[26–29] Utilizing measurements over a wide range of Cu thicknesses (50 – 200 nm) and annealing temperatures $T_A = 80 – 500$ °C, we show that the spin Kondo effect is clearly manifested in $\Delta R_{NL}(T)$ in Co/Cu NLSVs, despite the negligible $equilibrium$ solubility of Co in Cu.[30] The d dependence of ΔR_{NL} confirms that this is an interface effect, with only modest Co/Cu intermixing leading to low T suppression of α of up to 40 %. Most significantly, and with technological ramifications, the Kondo suppression of α in Co/Cu can extend to room temperature. Through complementary Scanning Transmission Electron Microscopy/Energy Dispersive X-ray Spectroscopy (STEM/EDX), we also describe and interpret a non-monotonic T_A dependence of the charge and spin Kondo effects. The suppression of spin accumulation at high T and the non-monotonic T_A dependence are in contrast with Fe/Cu NLSVs,[13] due to the larger T_K for Co in Cu, as well as the very different miscibilities of the two pairings.[30]

NLSVs [see Fig. 1(a) for device geometry] were fabricated on Si/Si-N substrates by ultra-high vacuum electron beam evaporation of high purity Co and Cu, multi-angle shadow evaporation[11,13,31,32] enabling single-shot deposition of low resistance (transparent) interfaces. The thickness t_N of the Cu channels ranged from 50 to 200 nm (with a width of 150 nm), while the Co thickness t_F was 16 nm (with widths of 100 to 150 nm). More details on fabrication, device characterization, and interface resistance appear in Supplementary Material (Figs. S1 and S2). Annealing was performed in vacuum ($\sim 10^{-8}$ Torr) for 2 hours at either 300 or 500 °C. Unannealed devices were exposed to $\sim$80 °C during lift-off, and are thus designated by $T_A = 80$ °C. Transport measurements were performed using a 13 Hz ac excitation of 316 μA in a continuous flow cryostat with a superconducting magnet.

Fig. 1(b) shows the channel resistivity $\rho_N(T)$ for three different t_N for illustrative T_A of 80 °C (solid lines) and 300 °C (dashed lines). The behavior is as expected, ρ_N decreasing with increasing t_N and upon annealing at 300 °C; the lowest ρ_N achieved is below 0.5 μΩ cm. $\Delta R_{NL}(T)$ was measured for a range of separations d from 150 – 2000 nm. Fig. 1(c) shows the results at d = 250 nm for both the T_A = 80 °C and 300 °C devices for the three t_N's studied. Note the clear non-monotonicity of $\Delta R_{NL}(T)$ for all t_N; the spin signal increases with decreasing T before reaching a maximum at T_{max} [arrows in Fig. 1(c)]. ΔR_{NL} then drops below T_{max}, with a decrease of up to 45 % (relative to the peak) by 5 K in annealed devices. T_{max} is notably dependent on T_A and t_N, increasing as T_A is increased to 300 °C, and as t_N is reduced. These features immediately suggest Kondo spin relaxation, the relatively high T_{max} potentially reflecting the high T_K for Co in Cu.

Looking in more detail, in these NLSVs ΔR_{NL} is T-dependent for two reasons. First, the effective polarization α_{eff} of the injected current varies due to the T dependence of the current polarization α_{FM} of the Co, as well as any spin-dependent processes at the FM/N interface. We thus use α_{eff} in place of α_{FM} to account for potential Kondo suppression at the interface.[13] Second, in the EY mechanism the spin relaxation rate scales with the T-dependent momentum relaxation rate, leading to T-dependent λ_N. We thus separate $\lambda_N(T)$ and $\alpha_{eff}(T)$ by fitting $\Delta R_{NL}(d,T)$ to a 1-D solution to the Valet-Fert model for NLSVs in the transparent limit:[33,34]

$$\Delta R_{NL} = \frac{4\,\alpha_{eff}{}^2 \dfrac{R_F{}^2}{\left(1 - \alpha_{eff}{}^2\right)^2 R_N} e^{-d/\lambda_N}}{\left(1 + 2\dfrac{R_F}{\left(1 - \alpha_{eff}{}^2\right) R_N}\right)^2 - e^{-2d/\lambda_N}}, \tag{1}$$

where $R_F = \rho_F \lambda_F / A_I$ and $R_N = \rho_N \lambda_N / A_N$ are the spin resistances of the FM and N. Here, A_I is the area of the FM/N interface, A_N is the channel cross-section, and all dimensions are measured by scanning electron microscopy. $\rho_N(T)$ is shown in Fig. 1(b), and the Co resistivity ρ_F is measured on nanowires with

identical dimensions to those in the NLSVs. We approximate the FM spin diffusion length $\lambda_F \approx 4$ nm, utilizing an empirical scaling relation[35] between λ_F and ρ_F (27 $\mu\Omega$ cm at 295 K in our case).[11]

Fitting for the only remaining parameters, λ_N and α_{eff}, distinguishes whether the low T suppressions in $\Delta R_{NL}(T)$ in Fig. 1(c) originate from spin relaxation throughout the channel [*i.e.*, in $\lambda_N(T)$], depolarization at the interface [*i.e.*, in $\alpha_{eff}(T)$], or both. Figs. 2(a-b) show $\Delta R_{NL}(d)$ at several T between 10 and 275 K for $t_N = 200$ nm and $T_A = 80$ and 300 °C. Fits to Eq. (1) are shown as solid lines. For $T_A = 80$ °C [Fig. 2(a)], $\Delta R_{NL}(d)$ is well-described by Eq. (1). For $T_A = 300$ °C [Fig. 2(b)], however, ΔR_{NL} at low d (≤ 350 nm) may potentially show slight deviations from Eq. (1), as seen in annealed Fe/Cu NLSVs and attributed to interfacial Kondo relaxation.[13] Nevertheless, from the high d behavior, annealing at 300 °C clearly increases λ_N, as indicated by the decreased slope of $\Delta R_{NL}(d)$ on this semi-log plot. Figs. 2(c-d) show the equivalent data for $t_N = 50$ nm for $T_A = 80$ and 300 °C. These lower t_N devices have reduced λ_N (as expected from ρ_N) and thus provide a smaller range of d over which ΔR_{NL} remains above the noise floor. This limits our ability to separate α_{eff} and λ_N in this limit. For this reason, we fit the results on the $t_N = 50$ nm, $T_A = 80$ °C, devices using a λ_N with a T dependence constrained by $1/\rho_N(T)$ (*via* EY scaling); $\lambda_N(T)$ indeed follows such scaling in higher t_N devices. More details are given in Supplementary Material (Fig. S3).

The primary results of this work are shown in Figs. 3(a-f), where we compare the extracted $\alpha_{eff}(T)$ and $\lambda_N(T)$ for all t_N and T_A. By normalizing $\alpha_{eff}(T)$ to its maximum, $\alpha_{eff,max}$, we compare the magnitude and onset T of the Kondo suppression of spin polarization as a function of t_N and T_A. Absolute values of $\alpha_{eff}(T)$ are given in Fig. S4 of Supplementary Material [Fig. S5 also provides normalized $\Delta R_{NL}(T)$ data for reference]. At $T_A = 80$ °C [black squares in Figs. 3(a-c)], $\alpha_{eff}(T)$ first increases upon cooling, before reaching a broad maximum and then dropping by $10 - 20$ % relative to $\alpha_{eff,max}$. Qualitatively, this is as anticipated from Fig. 1(c). At $T_A = 300$ °C, however [red circles in Figs. 3(a-c)], the behavior is different, α_{eff} continuously *decreasing* on cooling, such that by 5 K α_{eff} is suppressed by up to 40 % relative to

$\alpha_{eff,max}$. Increasing T_A to 500 °C [green triangles in Figs. 3(a–b)] then induces only small changes compared to 300 °C. The low T decrease in α_{eff} saturates at around 35 %, the $t_N = 100$ nm data even suggesting non-monotonic T_A dependence at low T.

Non-monotonicity with respect to T_A is also seen in λ_N [Figs. 3(d-f)], which first increases on annealing at 300 °C, before decreasing at 500 °C. At a given T_A, $\lambda_N(T)$ monotonically increases on cooling, however (as expected from EY relaxation), the only exception being $t_N = 200$ nm, $T_A = 300$ °C, where a small decrease occurs at low T. We thus conclude that the low T downturns in ΔR_{NL} in Fig. 1(c) are due to suppression of $\alpha_{eff}(T)$, as opposed to $\lambda_N(T)$, similar to other FM/N combinations studied by these means.[11,13] The additional spin relaxation at low T in Co/Cu NLSVs is therefore interfacial, deriving from Kondo spin relaxation at local moments near the FM/N interface. This is in contrast to naïve expectations based on equilibrium immiscibility of Co and Cu, as returned to below. Most significantly, at $T_A = 300$ °C we find no clear saturation or peak in $\alpha_{eff}(T)$, even up to 275 K. This indicates that the spin Kondo effect in Co/Cu NLSVs can be active even at room temperature. In contrast, prior studies of Kondo effects in NLSVs focused on FM/N pairings with T_K well below 300 K, such as Fe or Fe alloys with Cu ($T_K = 30\ K$)[6,8–13,15] or Ag ($T_K \approx 5$ K).[7,36,37]

As already noted, the low T suppression of $\alpha_{eff}(T)$ at $T_A = 500$ °C is similar to that at $T_A = 300$ °C, even evidencing non-monotonic T_A dependence. This is in contrast to Fe/Cu NLSVs, where Kondo effects strengthen monotonically with T_A.[13] To further understand this, we characterized these Co/Cu NLSVs using STEM/EDX to quantify Co/Cu intermixing. Figs. 4(a-c) show spatial maps of Co concentration C_{Co} in the x-z plane for $t_N = 200$ nm, acquired near the edge of a Co electrode (red signifies 100 % Co, blue 0 % Co). A fuller view is provided in Supplementary Material Fig. S2. To extract the interdiffusion length ℓ_{Co}, line scans of $C_{Co}(x)$ along the white lines shown in Figs. 4(a-c) were fit to a semi-infinite slab diffusion model, $C_{Co} \propto 1$- erf(x/ℓ_{Co}), where erf is the Gauss error function.[13] This results in $\ell_{Co} = 7.6 \pm 1$ nm for $T_A = 80$ °C. This is well above instrumental broadening, being similar, or even larger

than in as-deposited Fe/Cu ($\ell_{Fe} = 4.5$ nm).[13] This length remains unchanged within the uncertainty limits upon annealing to 300 °C [Fig. 4(b)]. At $T_A = 500$ °C, however, ℓ_{Co} *decreases* to 5.3 nm, accompanied by migration of Co across large length scales. The latter can be seen from the shape of the Co contact in Fig. 4(c), the tail that extends along the bottom of the channel (*i.e.*, the substrate interface) clearly retracting (back towards the FM nanowire) after 500 °C annealing, indicating segregation of Co from the Cu channel. While the decrease in ℓ_{Co} in Fig. 4(c) and the vanishing of the Kondo minimum in Fig. 4(f) suggest that this segregation occurs generally, the interfaces do clearly play a role, as is clear from the behavior of the Co "streak" at the Si-N interface in Figs. 4(a-c). Note also that vertical line scans in Figs. 4(a-c) (*i.e.*, along *z*) provide similar ℓ_{Co} *vs.* T_A trends to the horizontal line scans shown here.

These STEM/EDX findings also correlate with low *T* changes in $\rho_N(T)$ upon annealing, as shown in Fig. 4(d-f). This figure shows the sub-30-K *T* dependence of $(\rho_N - \rho_{min})/\rho_{min}$, where ρ_{min} is the minimum value of $\rho_N(T)$. The signature low-*T* upturn in $\rho_N(T)$ due to the charge Kondo effect is clear in the $t_N = 200$ nm, $T_A = 80$ °C devices [solid circles in Fig. 4(d)], signifying that *atomic-scale* magnetic impurities are indeed present in the bulk of the Cu channel. These data were fit to an empirical model for the Kondo effect:[38]

$$\rho_N = \rho_0 + AT^5 + \rho_K \left(\frac{T_K'^2}{T^2 + T_K'^2} \right)^s, \tag{2}$$

where ρ_0 is the residual resistivity, AT^5 captures electron-phonon scattering, ρ_K is the Kondo resistivity, and $T_K' = T_K/\sqrt{2^{1/s} - 1}$. For a spin ½ impurity, $s = 0.225$, but this is expected to decrease as the spin of the Kondo impurity increases.[39] In our case we obtain a good fit with $s = 0.07$, using the reported Co in bulk Cu T_K of 500 K.[26–29] The data are thus *consistent* with this high T_K, although, as always with high T_K systems, phonon scattering results in little sensitivity to the exact T_K. The extracted $\rho_K = 12$ nΩcm for $T_A = 80$ °C, increasing to 14 nΩcm for $T_A = 300$ °C [Fig. 4(e)], indicating increased C_{Co} in the channel. This is concurrent with strengthening of the spin Kondo effect in $\alpha_{eff}(T)$ [Figs. 3(a-c)]. At $T_A = 500$ °C, however

[Fig. 4(f)], the charge Kondo effect abruptly diminishes ($\rho_K = 1$ nΩcm), again indicating non-monotonic response to T_A.

Considering these STEM/EDX and $\rho_N(T)$ data, along with the trends in spin transport from Figs. 1(c) and 3(a-c), a consistent interpretation emerges. First, these as-deposited Co/Cu NLSVs must clearly contain kinetically-trapped Co atomic impurities, with non-negligible intermixing at the Co/Cu interface. $\alpha_{eff}(T)$ and ℓ_{Co} [Figs. 3(a) and 4(a)] show that this is true near the interface, $\rho_N(T)$ [Fig. 4(d)] demonstrating that C_{Co} must be non-negligible even deeper into the channel. This intermixing must derive from the *non-equilibrium* nature of the deposition. Although higher energy than evaporation, sputtering can result in Cu$_{1-x}$Co$_x$ solid solution films to remarkably high x.[40] We propose that similar effects occur here on a smaller scale, enabling Co/Cu mixing. Annealing at 300 °C increases diffusion, resulting in stronger charge [Figs. 4(d,e)] and spin [Figs. 3(a,b)] Kondo effects. At $T_A = 500$ °C, however, the dramatic changes signal a return to the equilibrium behavior (*i.e.*, Co/Cu segregation) that must occur at sufficiently high T_A.[41] STEM/EDX then shows segregation over large length scales [Fig. 4(c)], $\rho_N(T)$ indicating negligible charge Kondo effect [Fig. 4(f)]. ℓ_{Co} also decreases at this point, the low T Kondo suppression in $\alpha_{eff}(T)$ saturating, or even becoming non-monotonic with T_A. One final issue is the t_N dependence of these Kondo effects. For $t_N \leq 100$ nm the Kondo effect in $\rho_N(T)$ is negligible at all T_A [Figs. 4(d-f)], despite clear spin Kondo effects [Figs. 1(c) and 3(a-c)]. A potential explanation for this can be found in the literature on thin film dilute N$_{1-x}$FM$_x$ alloys, where weakening of the Kondo effect with decreasing thickness is widely reported,[42,43] and ascribed to spin-orbit-induced surface anisotropy. The fact that a pronounced spin Kondo effect remains in our Co/Cu NLSVs even at low t_N again highlights the sensitivity of this effect to the FM/N interface.

In conclusion, despite equilibrium immiscibility, Co/Cu NLSVs exhibit strong effects of Kondo spin relaxation due to interfacial intermixing. These reach a maximum at 300 °C annealing, at which point the Kondo suppression of the effective injected spin current polarization is as much as 40 %, persisting even to room temperature, with clear technological implications. Elimination of this effect could employ

an N channel or FM/N interlayer metal that does not support local magnetic moments, such as Al. Finally, the spin and charge Kondo effects in these devices exhibit complex trends with channel thickness and annealing temperature, which can be interpreted in terms of the interplay between Co/Cu diffusion kinetics and thermodynamics, and the known thickness dependence of the charge Kondo effect.

See supplementary material for additional details on device fabrication and characterization, absolute spin polarizations, and normalized spin signals, as well as a discussion of fitting procedures for 50-nm-thick channels.

References

[1] M. Johnson and R.H. Silsbee, Phys. Rev. Lett. **55**, 1790 (1985).

[2] F.J. Jedema, A.T. Filip, and B.J. van Wees, Nature **410**, 345 (2001).

[3] M. Takagishi, K. Yamada, H. Iwasaki, H.N. Fuke, and S. Hashimoto, IEEE Trans. Magn. **46**, 2086 (2010).

[4] Y.K. Takahashi, S. Kasai, S. Hirayama, S. Mitani, and K. Hono, Appl. Phys. Lett. **100**, 52405 (2012).

[5] M. Yamada, D. Sato, N. Yoshida, M. Sato, K. Meguro, and S. Ogawa, IEEE Trans. Magn. **49**, 713 (2013).

[6] T. Kimura, T. Sato, and Y. Otani, Phys. Rev. Lett. **100**, 66602 (2008).

[7] G. Mihajlović, J.E. Pearson, S.D. Bader, and A. Hoffmann, Phys. Rev. Lett. **104**, 237202 (2010).

[8] H. Zou and Y. Ji, Appl. Phys. Lett. **101**, 82401 (2012).

[9] E. Villamor, M. Isasa, L.E. Hueso, and F. Casanova, Phys. Rev. B **87**, 94417 (2013).

[10] N. Motzko, N. Richter, B. Burkhardt, R. Reeve, P. Laczkowski, L. Vila, J.-P. Attané, and M. Kläui, Phys. Status Solidi **211**, 986 (2014).

[11] L. O'Brien, M.J. Erickson, D. Spivak, H. Ambaye, R.J. Goyette, V. Lauter, P.A. Crowell, and C. Leighton, Nat. Commun. **5**, 3927 (2014).

[12] J.T. Batley, M.C. Rosamond, M. Ali, E.H. Linfield, G. Burnell, and B.J. Hickey, Phys. Rev. B **92**, 220420 (2015).

[13] L. O'Brien, D. Spivak, J.S. Jeong, K.A. Mkhoyan, P.A. Crowell, and C. Leighton, Phys. Rev. B **93**, 14413 (2016).

[14] Ikhtiar, S. Kasai, Y.K. Takahashi, T. Furubayashi, S. Mitani, and K. Hono, Appl. Phys. Lett. **108**, 62401 (2016).

[15] E. Villamor, M. Isasa, L.E. Hueso, and F. Casanova, Phys. Rev. B **88**, 184411 (2013).

[16] K. Hamaya, T. Kurokawa, S. Oki, S. Yamada, T. Kanashima, and T. Taniyama, Phys. Rev. B **94**, 140401 (2016).

[17] F. Casanova, A. Sharoni, M. Erekhinsky, and I.K. Schuller, Phys. Rev. B **79**, 184415 (2009).

[18] M. Erekhinsky, F. Casanova, I.K. Schuller, and A. Sharoni, Appl. Phys. Lett. **100**, 212401 (2012).

[19] R.J. Elliott, Phys. Rev. **96**, 266 (1954).

[20] Y. Yafet, in *Solid State Phys.*, edited by F. Seitz and D. Turnbull (Academic, New York, 1963), pp. 1–98.

[21] F. Beuneu and P. Monod, Phys. Rev. B **13**, 3424 (1976).

[22] J. Kondo, Prog. Theor. Phys. **32**, 37 (1964).

[23] K.-W. Kim, L. O'Brien, P.A. Crowell, C. Leighton, and M.D. Stiles, Phys. Rev. B **95**, 104404 (2017).

[24] P.W. Anderson, Phys. Rev. **124**, 41 (1961).

[25] J. Friedel, Nuovo Cim. **7**, 287 (1958).

[26] M.D. Daybell and W.A. Steyert, Rev. Mod. Phys. **40**, 380 (1968).

[27] C.A. Domenicali and E.L. Christenson, J. Appl. Phys. **32**, 2450 (1961).

[28] R. Tournier and A. Blandin, Phys. Rev. Lett. **24**, 397 (1970).

[29] H. Prüser, M. Wenderoth, P.E. Dargel, A. Weismann, R. Peters, T. Pruschke, and R.G. Ulbrich, Nat.

Phys. **7**, 203 (2011).

[30] T. Nishizawa and K. Ishida, Bull. Alloy Phase Diagrams **5**, 161 (1984).

[31] F.J. Jedema, M. V. Costache, H.B. Heersche, J.J.A. Baselmans, and B.J. van Wees, Appl. Phys. Lett. **81**, 5162 (2002).

[32] Y. Ji, A. Hoffmann, J.S. Jiang, J.E. Pearson, and S.D. Bader, J. Phys. D. Appl. Phys. **40**, 1280 (2007).

[33] T. Valet and A. Fert, Phys. Rev. B **48**, 7099 (1993).

[34] S. Takahashi and S. Maekawa, Phys. Rev. B **67**, 52409 (2003).

[35] J. Bass and W.P. Pratt, J. Phys. Condens. Matter **19**, 183201 (2007).

[36] H. Idzuchi, Y. Fukuma, L. Wang, and Y. Otani, Appl. Phys. Lett. **101**, 22415 (2012).

[37] G. Mihajlović, D.K. Schreiber, Y. Liu, J.E. Pearson, S.D. Bader, A.K. Petford-Long, and A. Hoffmann, Appl. Phys. Lett. **97**, 112502 (2010).

[38] D. Goldhaber-Gordon, J. Göres, M.A. Kastner, H. Shtrikman, D. Mahalu, and U. Meirav, Phys. Rev. Lett. **81**, 5225 (1998).

[39] T.A. Costi, L. Bergqvist, A. Weichselbaum, J. von Delft, T. Micklitz, A. Rosch, P. Mavropoulos, P.H. Dederichs, F. Mallet, L. Saminadayar, and C. Bäuerle, Phys. Rev. Lett. **102**, 56802 (2009).

[40] J.R. Childress and C.L. Chien, Phys. Rev. B **43**, 8089 (1991).

[41] V. Zhukova, J. Mino, J.J. Del Val, M. Ipatov, R. Varga, M.N. Baibich, G. Martinez, A. Granovsky, and A. Zhukov, J. Supercond. Nov. Magn. **30**, 1109 (2017).

[42] O. Újsághy, L. Borda, and A. Zawadowski, J. Appl. Phys. **87**, 6083 (2000).

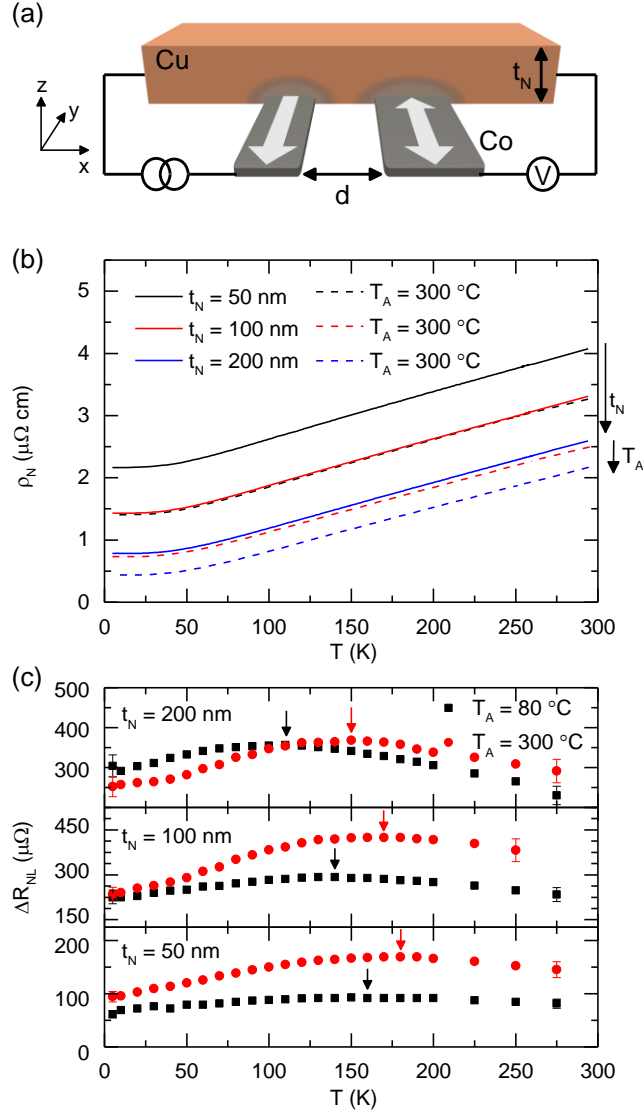[43] O. Újsághy and A. Zawadowski, J. Phys. Soc. Japan **74**, 80 (2005).

FIG. 1. (a) Non-local spin valve geometry, showing the Cu channel (thickness t_N), Co injector/detector (separation d), and measurement configuration; exaggerated intermixing is shown. White arrows illustrate the toggling of the Co magnetization to the parallel and anti-parallel states. (b) Temperature (T) dependence of the resistivity (ρ_N) of Cu channels, as-deposited ($T_A = 80\ °C$) and after annealing at $T_A = 300\ °C$, for t_N = 50, 100 and 200 nm. (c) T dependence of the spin accumulation signal (ΔR_{NL}) for t_N = 200, 100 and 50 nm, as-deposited ($T_A = 80\ °C$) and after annealing at $T_A = 300\ °C$. In all cases $d = 250$ nm. Arrows indicate maxima in $\Delta R_{NL}(T)$.
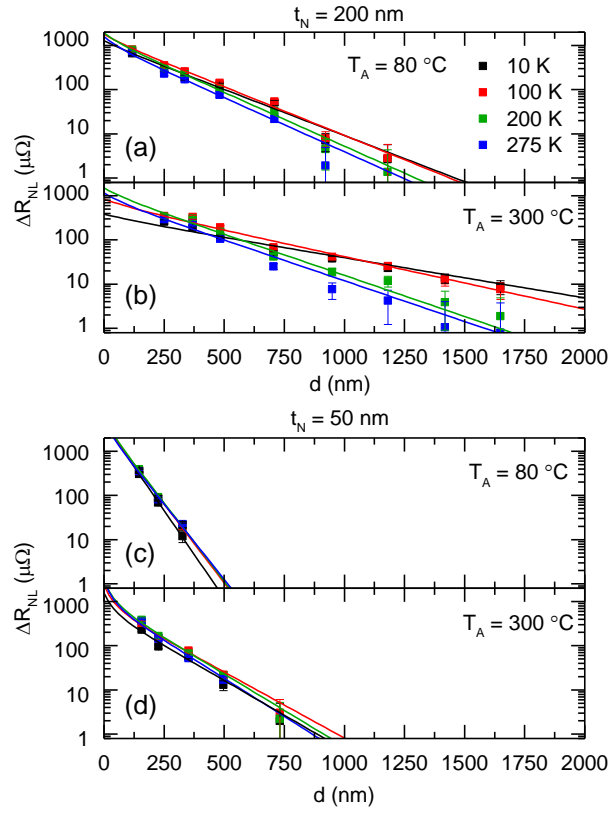
FIG. 2. Spin accumulation signal $\Delta R_{NL}(T)$ *vs.* the injector/detector separation d for channels of thickness $t_N = 200$ nm (top panels) and 50 nm (bottom panels). Data shown for as-deposited [$T_A = 80$ °C, (a,c)], and after annealing at $T_A = 300$ °C (b,d), at multiple measurement T between 10 and 275 K. Solid lines are fits to Eq. (1).
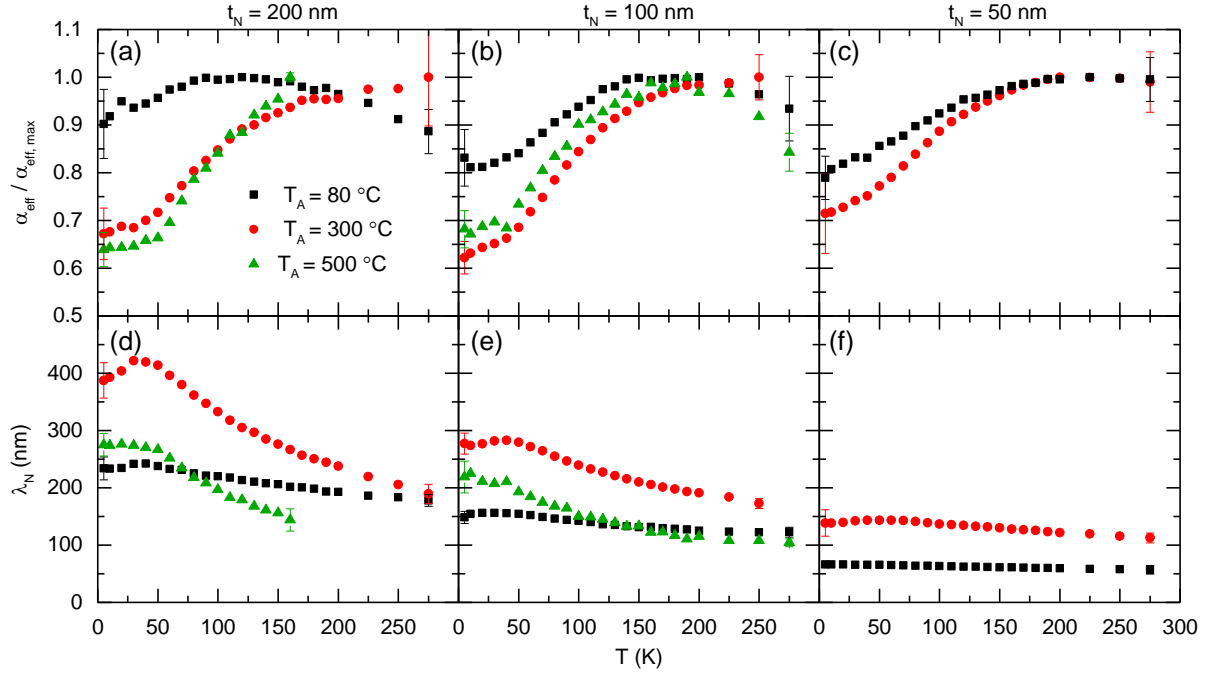
FIG. 3. Temperature (T) dependence of the effective injected spin polarization normalized to its maximum ($\alpha_{eff}/\alpha_{eff,max}$, top panels) and the spin diffusion length in the non-magnetic channel (λ_N, bottom panels). Data are shown for channel thicknesses (t_N) of 200 nm (left), 100 nm (middle), and 50 nm (right). Results for $T_A = 80$, 300 and 500 °C are shown. First and last data points show representative error bars on each data set.
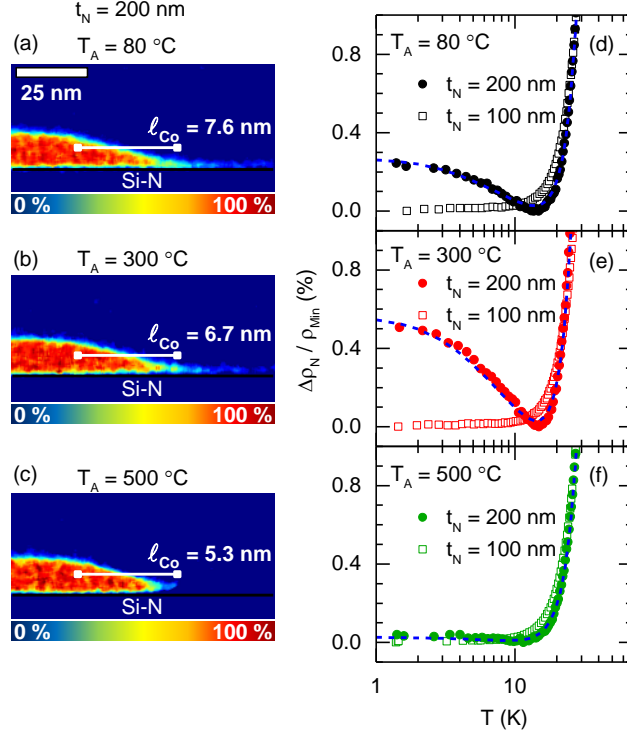
FIG. 4. (a-c) Spatial maps of Co atomic concentration (C_{Co}) in the x-z plane [see coordinate system in Fig. 1(a)] for $T_A = 80$, 300 and 500 °C devices. Red signifies $C_{Co} = 100$ %, blue $C_{Co} = 0$ %. The interdiffusion length, ℓ_{Co}, is found by fitting $C_{Co}(x)$ along the white lines to the semi-infinite slab diffusion model. (d-f) Temperature (T) dependence (log scale) of the resistivity for Cu channel thicknesses (t_N) of 100 and 200 nm normalized to their minimum value, $(\rho_N - \rho_{Min})/\rho_{Min}$, for $T_A = 80$, 300 and 500 °C. Results are shown for injector/detector separations (d) of 250 nm. Blue dashed lines are fits to Eq. (2). Note the absence of a Kondo minimum in all $t_N = 100$ nm data, which, can be interpreted in terms of prior work on thin film Kondo systems.